Atomic Force Microscopy Imaging and Fractal Analysis of Surface Roughness of Polyvinyl alcohol-Chitosan Films

Ganna Kovtun
Laboratry of biosensors,
Institute of Magnetism NAS of Ukraine and MES of Ukraine
Kyiv, Ukraine
Group of Nanotechnology and Materials,
Mining and Industrial Engineering School of Almaden, University of Castilla-La Mancha,
Almadén, Spain
anna-kovtun@ukr.net

David Casas
Group of Nanotechnology and Materials,
Mining and Industrial Engineering School of Almaden, University of Castilla-La Mancha
Almadén, Spain
david.casas@uclm.es

Teresa Cuberes
Group of Nanotechnology and Materials,
Mining and Industrial Engineering School of Almaden, University of Castilla-La Mancha
Almadén, Spain
teresa.cuberes@uclm.es

Atomic Force Microscopy Imaging and Fractal Analysis of Surface Roughness of Polyvinyl Alcohol–Chitosan Films, Proceedings of the 2024 IEEE International Conference on Electronics and Nanotechnology (ELNANO), Kviv, Ukraine, 2024, pp 261-265
DOI: 10.1109/ELNANO63394.2024.10756913.
The final published version is available at IEEE Xplore:
https://ieeexplore.ieee.org/document/10756913

Abstract—Polyvinyl alcohol (PVA)-Chitosan films were studied by thermogravimetric analysis (TGA), atomic force microscopy (AFM), ultrasonic force microscopy (UFM) and lateral force microscopy (LFM) and the results were compared to those of pure PVA and pure chitosan films. The surface of PVA-chitosan blends consists of small, rounded clusters, and random pores, but in contrast to the individual component films, inhomogeneous features were observed on the surface, in the form of relatively large higher clusters, which gave rise to lower elastic and frictional contrast. In addition, UFM and LFM revealed the presence of softer and lower friction regions which

could not be distinguished in the topographic images. Such areas may be related to the formation of a new different phase as a result of PVA-chitosan interactions. TGA confirmed an increase in the thermal stability of the PVA-chitosan blend compared to the individual component films. The dependence of the root mean square (RMS) roughness on length scale was investigated. It was shown that the PVA-chitosan film has a higher RMS roughness for shorter measured lengths than the pure PVA samples, but the roughness for long measured lengths is lower than in pure PVA samples, which is explained by the lower Hurst number of the PVA-chitosan blend. The Hurst exponent and fractal dimension of the samples were obtained, which indicate a higher level of fractality and a more irregular shape of the surface topography for the PVA-chitosan films.

Keywords—polyvinyl alcohol, chitosan, AFM, roughness, ultrasonic force microscopy, lateral force microscopy

I. INTRODUCTION

Development of materials with film forming capacity is of growing interest. Polymeric films are widely used in the creation of sensing materials, drug delivery systems, wound dressings, packaging applications, recovery of organic and inorganic pollutants, etc. Polymeric blends represent a class of materials with better mechanical, thermal, biocompatibility, etc. properties than the individual components.

Chitosan is a natural polysaccharide, a deacetylated derivative of chitin (Fig. 1). Biocompatibility, non-toxicity, antioxidant and antimicrobial activity, the ability to biodegrade and the presence of active functional groups allow chitosan to be used in the food industry, cosmetology, biomedical and synthetic purposes, for example, in the microencapsulation of substances to prolong their action [1], in the production of foams [2], emulsions [3], films for different applications [4], etc. However, chitosan films have some disadvantages for example poor mechanical properties, especially brittleness, low elasticity, and low resistance to water, which limit the use of this type of film. Therefore, another polymers, crosslinking agents and nanomaterials are used to improve the thermal, mechanical and gas barrier properties without hindering their biodegradable and non-toxic character. For example, PVA, a biodegradable, synthetic polymer, has excellent film forming properties and can be blended with different synthetic and natural polymers. Due to its biocompatibility, PVA is used to produce hydrogels for biomedical use, including in combination with chitosan. Blends of chitosan and PVA are attracting a lot of attention from researchers to create new materials for biomedical and industrial applications [5, 6].

The structure of polymer matrices plays an important role in the creation of materials with controlled properties. Surface topography is known to substantially influence the properties of a material, such as adhesion, adsorption, optical response, biocompatibility etc. AFM constitutes a unique tool to provide information on the materials properties on the nanoscale. Based on the measurement of the forces experienced by a nanometric tip located at the end of a micro-cantilever, the technique can be used for the measurement of the topography of surfaces with nanometer scale resolution, as well as for the mechanical, electrical, magnetic, or frictional response of nanomaterials or nanoscale material domains. Recently, a new family of AFM procedures based on the use of ultrasound is being developed [7, 8]. Techniques such as UFM, based on the so-called mechanical-diode effect, have already demonstrated the capability to differentiate nanoscale regions on the basis of their elastic and adhesive properties, as well as to provide subsurface materials information [9, 10].

There are only few works in the literature related to study of PVA/chitosan films with AFM [11,12]. In [11,12] the microstructure of PVA/chitosan films, and their modification by the addition of an ionic liquid to the blend, has been

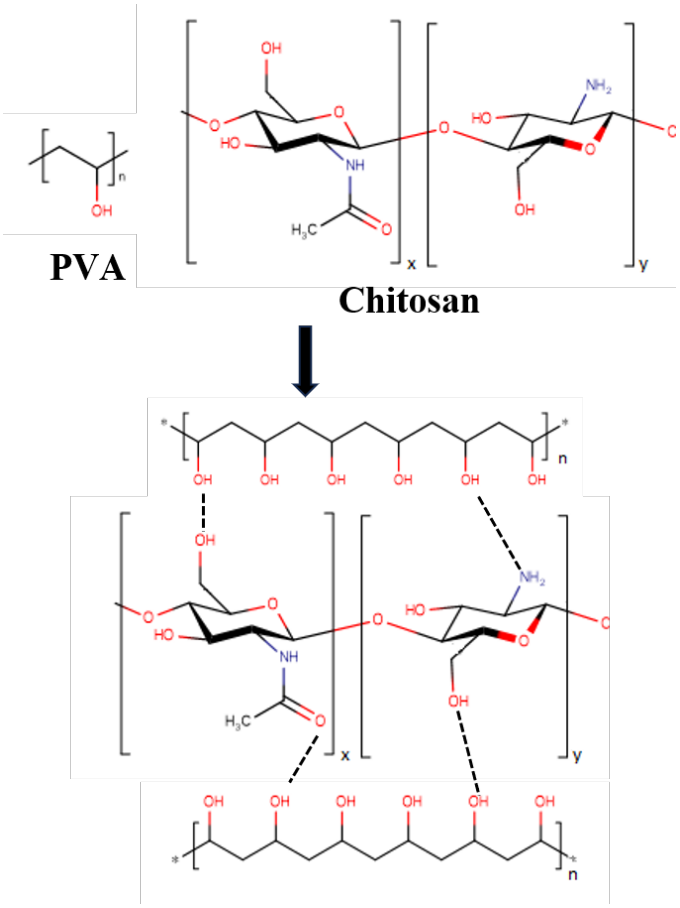

Fig. 1. Structure of PVA, chitosan and the possible interactions in PVA-chitosan matrix.

studied with AFM. Based on their findings, the beneficial influence of ionic liquid addition on the film's properties, and the formation of a network structure due to the intermolecular forces between the constituents could be concluded. Their results indicated major differences in the polymer films surface morphology. However, to the best of our knowledge, no report has yet been published on the study of the nanoscale frictional and elastic properties of PVA-chitosan films. Only the root mean square roughness, which is a common measure of surface morphology and characterizes the profile of the analysed surface, was used for analysis of the surface topography of PVA-chitosan films. But the RMS roughness does not take into account the distance between the features on the surface, and it is highly dependent on the length scale of observation [13]. Thus, fractal analysis can be used for a more accurate description because it considers the importance of the scale of measurement with respect to structural features.

The aim of this paper is to investigate the impact of the molecular interactions in PVA-chitosan blends using advanced AFM- based procedures, such as UFM, LFM and fractal analysis of the surface roughness. The results were complemented with TGA data.

II. EXPERIMENTAL

A. Materials and sample preparation.

Polyvinyl alcohol (Mw 31 000-50 000 g/mol, 98-99% hydrolysed, Sigma Aldrich), chitosan (Mw 75 kDa, degree of deacetylation 70%) and glacial acetic acid (Sigma Aldrich) were used in this paper.

PVA was dissolved in distilled water with stirring at 90 °C when heated in a water bath for 2 hours, 400 rpm, to prepare 7 wt.% stock solution. Chitosan stock solution was prepared by dissolving chitosan in a 2% (v/v) aqueous acetic acid solution at a concentration of 2 wt.% with stirring at 40ºC, 400 rpm, 3h, then it was left to stand overnight at room temperature, followed by centrifuging to remove the insoluble material. Mixed PVA-chitosan solution with 3.5 wt.% PVA and 0.65 wt.% chitosan was prepared from above stock polymer solutions by adding distilled water to the corresponding amounts, stirring at 40ºC, 400 rpm, 30 min.

The polymer films were prepared by solution casting method. Solutions of PVA, chitosan and PVA-chitosan mixture were poured on polystyrene petri dishes and dried at room temperature (20-25°C) and ambient humidity ~ 50% R.H.

B Thermogravimetric Analysis (TGA).

The thermal behaviour of the samples was examined using the DTA (Differential Thermal Analysis)-TGA equipment (Setaram, France). Thermograms were made in an air atmosphere in the temperature range of 20°C to 500 °C with a heating rate of 5 ºC/min and in a Pt crucible. Derivative thermogravimetric (DTG) analysis was performed to identify the thermal transformation peaks.

C Scanning Probe Microscopy.

Contact-mode AFM, LFM and UFM were performed using a NANOTEC instrument (Madrid, Spain), appropriately modified for UFM measurements [7]. For UFM, ultrasonic frequencies of ~3.8 MHz and modulation frequencies of 2.4 KHz were applied from a piezoelectric element placed under the sample. Typically, Olympus Silicon Nitride cantilevers with a nominal spring constant of 0.06 N/m and a nominal tip radius of 20 nm were used. The measurements were performed in air, at ambient conditions (20-25°C, ~ 35% R.H.). The root mean square roughness analysis was performed with WSxM software (Madrid, Spain) [14].

III. RESULTS AND DISCUSSION

The thermal stability, degradation stages, moisture content of PVA, chitosan, and PVA-chitosan films were studied by thermogravimetric analysis. Figure 2 shows the curves of mass loss against temperature (TG) and its derivative (DTG) for the PVA, chitosan and PVA-chitosan films. DTG curve is useful to distinguish overlapping mass loss events, to identify shapes and maxima of mass loss processes, and to help identify minor mass loss steps. Each DTG peak represents a separate event and indicates the maximum rate of mass loss.

Thermal transformations of the pure PVA film occur in 4 main stages (Fig. 2a, b): the loss of physically absorbed water; partial dehydration of PVA accompanied by polyene formation; polyene decomposition; thermo-oxidation of carbonized residue [15, 16]. The mass losses are 5.2 %, 60 %, 16.1 %, 10.3 % for degradation stages from 1st to 4th respectively.

The TGA data for the pure chitosan show two steps in weight loss in the studied temperature range. The mass loss for the first step with maximum rate of mass loss of 8% is at 106 °C and can be associated with the loss of adsorbed water. The second step with maximum rate of mass loss of 280 °C is characterized by 45 % mass loss and is connected with deacetylation and depolymerization of chitosan [17].

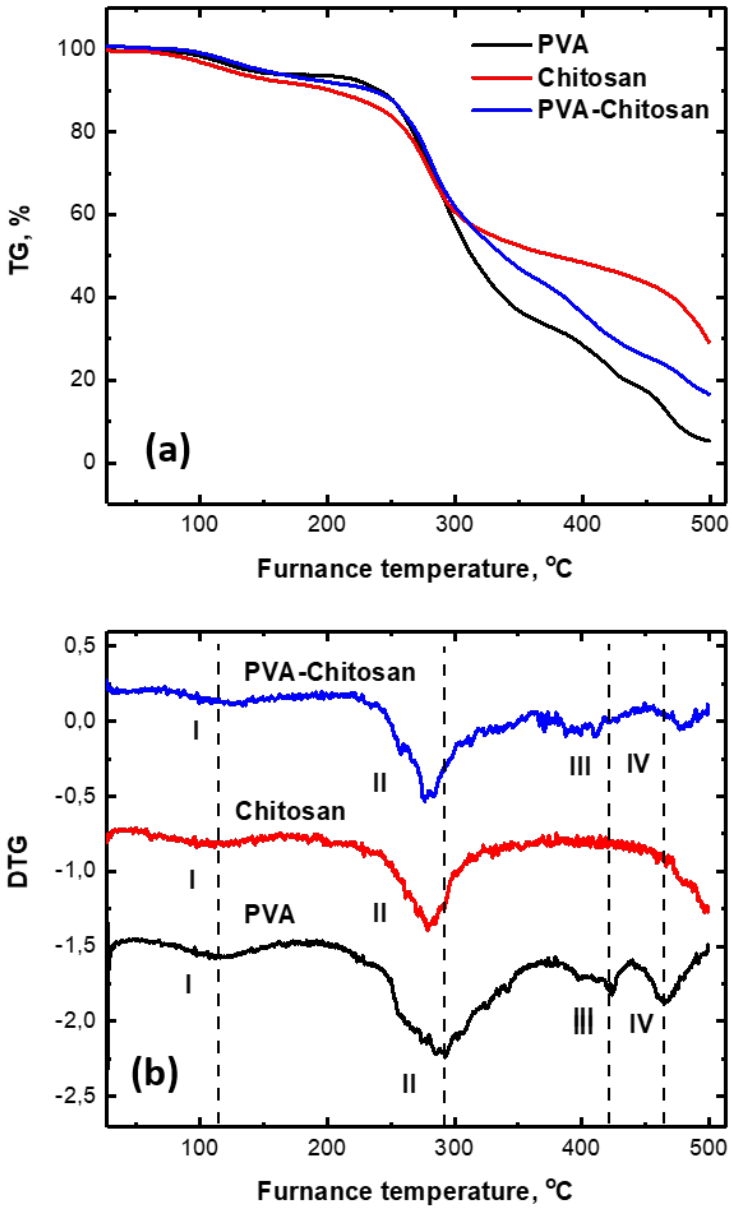

Fig. 2. TG (a), DTG (b) curves of PVA, chitosan and PVA-chitosan films.

Thermal transformations of PVA-chitosan blend occur in 4 stages similarly to pure PVA film, but mass losses and positions of DTG peaks change a little bit. The mass losses for degradation stages from 1st to 4th are the following: 9 %, 49 %, 17 %, 9 %. So, PVA-chitosan blend contains more adsorbed water in comparison to pure PVA film. Moreover, the temperature related to the highest rate of mass loss on this stage shifts to higher temperatures (128 °C in comparison with 118 °C for pure PVA and 106 °C for pure chitosan). The initial decomposition temperature of the blend increases to 252 °C in comparison to 241 °C for PVA and 245 °C for chitosan. So, PVA-chitosan film is

characterised by higher thermal stability. The second peak on the DTG curve shifts slightly to lower temperatures (280 °C in comparison to 290 °C for pure PVA), this can be caused by presence of chitosan, which also has a DTG peak at this temperature. The third peak on DTG curve is also slightly shifted to lower temperature, but the fourth peak is shifted to higher temperature (480 °C in comparison to 465 °C for pure PVA). The mass losses for last three stages decrease in comparison with pure PVA. Possible formation of hydrogen bonds between -OH groups of PVA and -OH and -NH_2 groups of chitosan (Fig. 1) can result in increase of thermal stability of polymer blend.

Fig. 3 shows topography in AFM contact mode for PVA (a) and chitosan (b) films. Pure chitosan and PVA films indicate quite homogeneous surfaces with round clusters and irregular pores of nanoscale size. Clusters with sizes of about 50-60 nm in diameter and pores of about 60-70 nm can be distinguished for PVA films. Clusters with sizes of about 75 nm in diameter and pores of about 70 nm can be distinguished for chitosan films. Both samples are characterised by homogeneous contrast in LFM and UFM images (not shown here). Fig. 3 (c, d) show contour lines along the arrows in (a, b) for PVA and chitosan films respectively. The height variations for PVA film are about of 10 nm, while for chitosan films slightly higher heights (up to 14 nm) were observed.

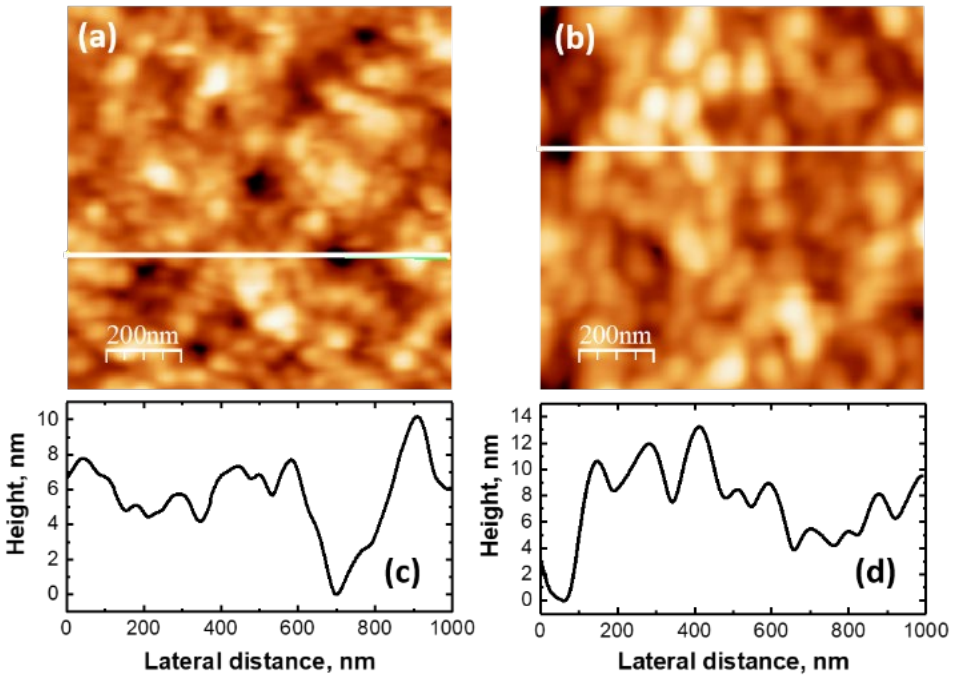

Fig. 3 Topography in AFM contact-mode of PVA (a) and chitosan (b) films; (c, d) contour line along the arrow in (a, b) for PVA and chitosan films respectively.

Surface topography of PVA-chitosan film is presented on Fig. 4 (a). It can be seen that surface is formed by small, rounded shape clusters of about 40 nm size and random pores, but in contrast to films of the individual components, some features (clusters) appear with higher height (like those enclosed by a circle in Fig. 4(a)).

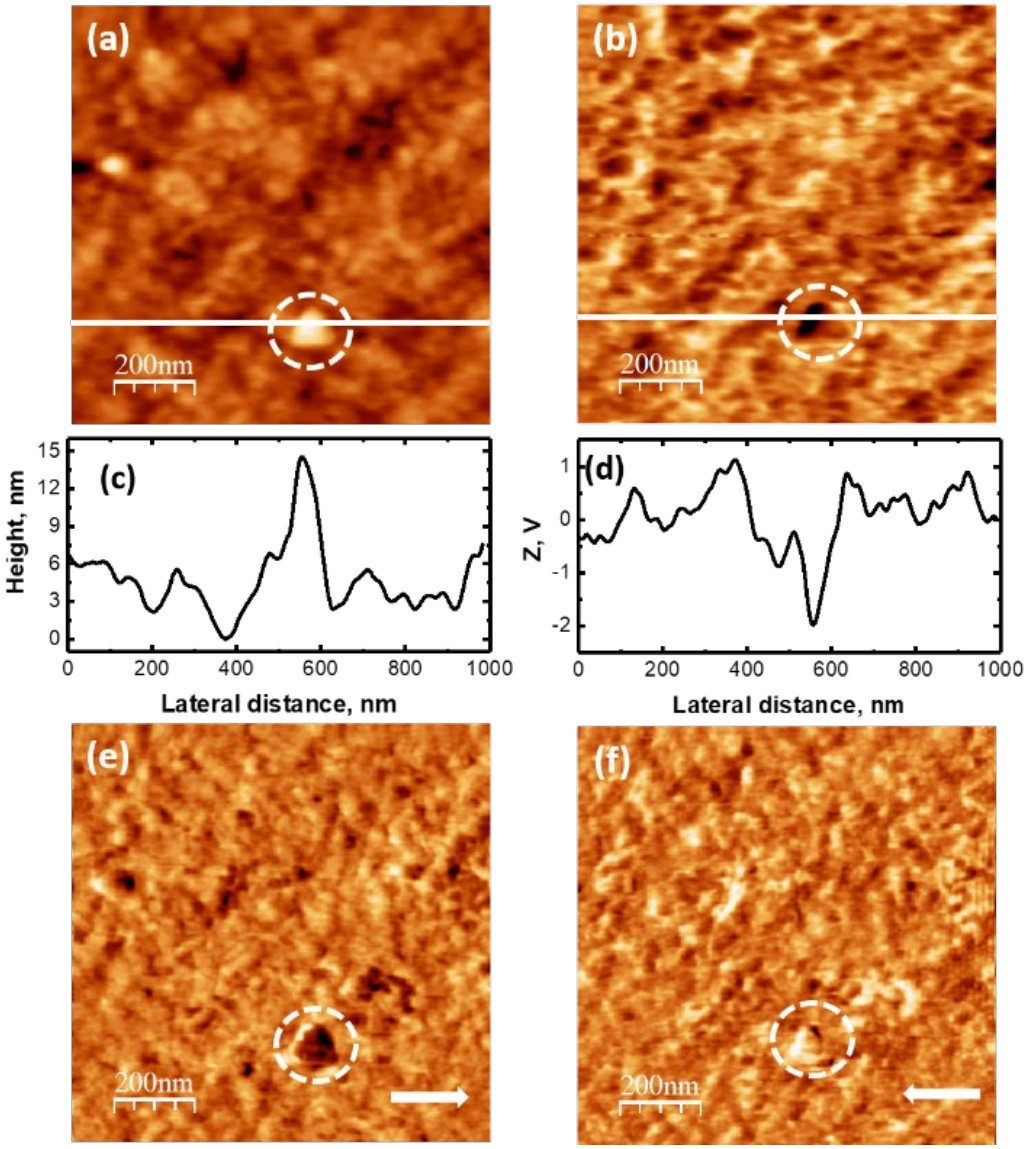

Fig 4. (a) Topography in AFM contact-mode; (b) UFM image recorded immediately after over the same surface area for PVA-chitosan film; (c, d) - contour line along the arrow in (a, b) for topography and UFM respectively. (e, f) LFM scanning from left to right (e) and from right to left (f).

The surface topographic height varies approximately from 0 to 6 nm; however, at the aforementioned features it reaches about 15 nm (Fig. 4 (c)). On the Fig. 4 (b) clusters with different UFM contrast are noticeable. Some of them have darker contrast, and some have stiffer (brighter) contrast (Fig. 4 (b, d)). The area with a higher topographic height, (enclosed by circles in Fig. 4(a-f)) yield lower frictional contrast in LFM and softer contrast in UFM. Hence, this region has different structure than the surrounding film, which can possibly be caused by chitosan enrichment.

Fig. 5 shows the contact-mode AFM surface topography, LFM and UFM images for PVA-chitosan film recorded on a nearby region of bigger size (5 μm *5 μm). Here we find extended regions with lower frictional contrast in LFM and softer contrast in UFM like those enclosed by dashed rectangles (Fig. 5 b-d). In this case there is no characteristic topographic feature related to the areas with lower friction and lower UFM contrast. These regions may arise due to formation of a distinct PVA-chitosan phase. Hydroxy groups of

PVA can form hydrogen bonds with hydroxy and amino groups of chitosan (Fig. 1), and excess chitosan may lead to formation of a distinct phase with different properties.

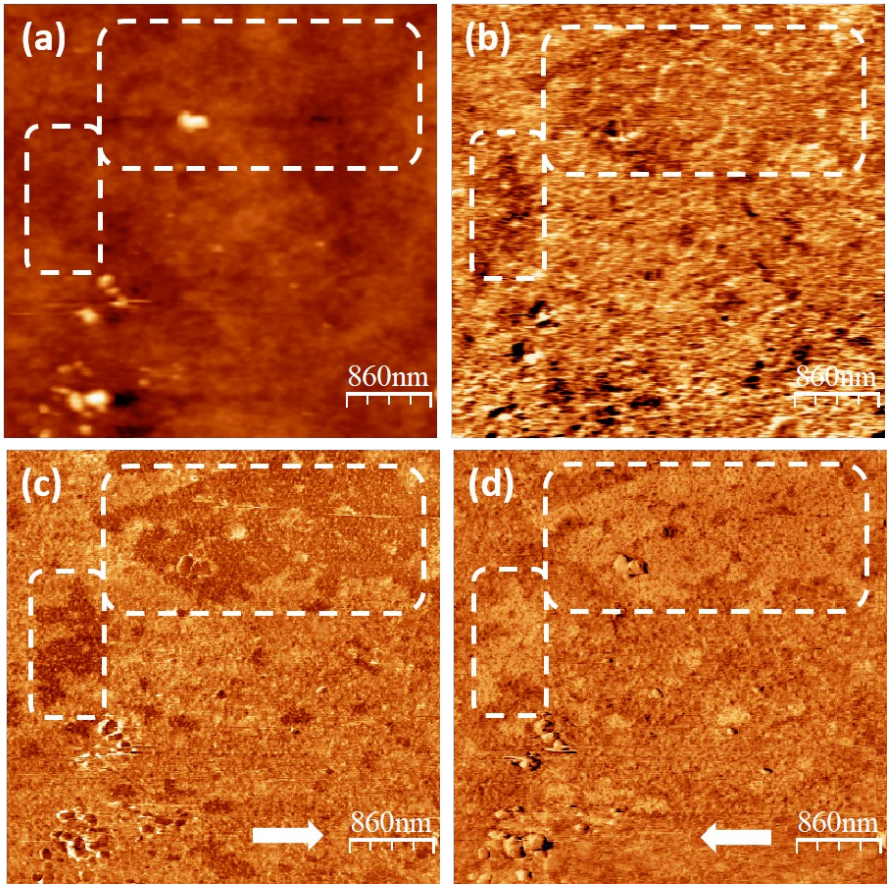

Fig. 5. PVA-chitosan film. (a) Contact-mode AFM surface topography. (b) UFM recorded immediately after (a) over the same surface area and (c, d) LFM recorded scanning from left to right (c) and from right to left (d).

The root mean square roughness (Rq) is the root mean square height of the surface around some mean value. It characterizes the profile of the analysed surface, its peaks and valleys, and depends on the length scale of observation. Self-affine surfaces have roughness characteristics which scale according to a power law [18]. The relationship between Rq and the length scale of measurements is given by the relationship

$$R_q = aL_0^H \qquad (1)$$

where H is the Hurst exponent, L_0 is the measurement length and a is an arbitrary constant.

For AFM images which were made across a large range of scan sizes the Hurst exponent can be obtained from the slope of a plot of the natural logs of R_q versus L_0

$$\mathrm{H} = d(\log_{10}R_q)/d(\log_{10}L_0) \qquad (2)$$

The Hurst exponent is related to the fractal dimension (D_f) by the relationship

$$D_f = n + 1 - H \qquad (3)$$

where n+1 is the dimension of embedded space (n=1 for a profile, n=2 for a plane).

The dependences of the natural logs of R_q versus the natural logs L_0 for PVA, chitosan and PVA-chitosan films are presented in the Fig. 6. From these plots the Hurst exponent and the fractal dimension of the samples were obtained, and the summarized parameters are given in the table 1. The PVA film has a Hurst exponent in the region $0.5<H<1$, which means an inhomogeneous distribution of roughness, while chitosan and PVA-chitosan films are characterised by homogeneous distribution of roughness ($0<H<0.5$) with increasing scan size. The fractal dimension increases for chitosan and PVA-chitosan films in comparison with pure PVA film. The fractal dimension of a surface varies in the range $2 \leq D_f \leq 3$; hence, the addition of chitosan to PVA leads to a more complex, "3D-like", surface topographic structure [19].

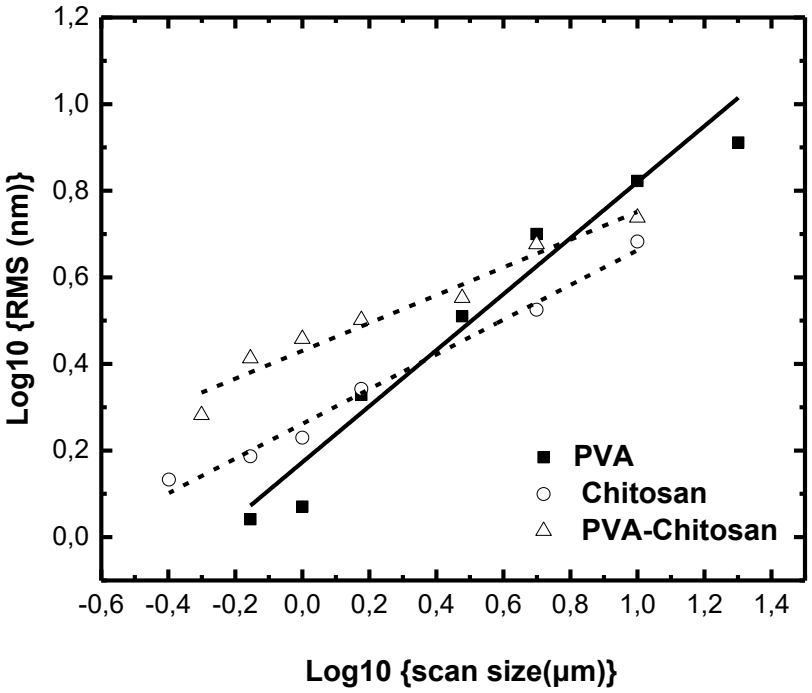

Fig. 6 (a) Plot of the natural logs of R_q versus natural logs L_0 for PVA, chitosan and PVA-chitosan films

As it can be seen from Fig. 6, the RMS roughness of the PVA-chitosan film is higher than this of the pure PVA film for the smaller measured lengths, and lower for larger measured lengths (larger scanning sizes), as a result of the different Hurst exponents of the films (i.e. difference in slope for both sample types), which indicates their different fractal dimensions.

Polymer molecules can adopt different conformations, their molecular size itself may influence the surface topography and roughness; interactions between PVA and chitosan may also increase the surface structural complexity, while the RMS surface roughness will be dependent on the sampled area.

TABLE I. VALUES OF HURST EXPONENT (H), FRACTAL DIMENSION (D_F), RMS ROUGHNESS (R_Q), SKEWNESS (S) AND KURTOSIS (K) FOR PVA, CHITOSAN AND PVA-CHITOSAN FILMS.

No.	Sample	H	D_f	R_q (10μm)	S (10μm)	K (10μm)
1	PVA	0.65	2.35	6.65	0.03	2.98
2	Chitosan	0.40	2.60	4.81	0.37	3.28
3	PVA-chitosan	0.32	2.68	5.45	0.34	6.61

To further characterize the films surface structure parameters such as the skewness (S) and the kurtosis (K) were calculated for 10μm*10μm images (table 1). The skewness measures the asymmetry of the (non-)Gaussian distribution of the roughness profile over its midline, being therefore sensitive to the presence of deep depressions or high peaks. A symmetric distribution is reflected in zero skewness. Predominant profiles of peaks above a flatter average are reflected in positive skewness, while negative skewness refers to profiles prevalent in deep valleys. Kurtosis describes the probability of flattening the profile. Kurtosis is less than 3 for surfaces with relatively flat peaks and valleys, and a kurtosis is above 3 for surfaces with sharp peaks and valleys [20]. It can be seen from table 1 that films of individual PVA and chitosan are characterized by kurtosis values close to 3, that means almost perfectly random surface. While the nanostructure of mixed PVA-chitosan film is defined by appearance of sharp peaks and valleys. All studied samples have positive skewness values, however for PVA film this value is much closer to zero, indicating almost symmetric distribution of peaks and valleys.

CONCLUSIONS

Summarizing, scanning probe microscopy was applied to characterize PVA-chitosan films. The surface of PVA- chitosan blends is formed by rounded shape clusters and random pores. Also, some characteristic features were observed over the surface, in the form of relatively big higher clusters, which gave rise to lower elastic and frictional contrast. In addition, LFM and UFM revealed the presence of softer and lower friction regions which could not be distinguished in the topography images. Such inhomogeneous areas may be related to formation of a new different phase as a result of PVA-chitosan interactions. TGA analysis confirmed an increase in the thermal stability of the PVA-chitosan blend compared to the individual component films. The RMS roughness of the PVA-chitosan film has higher values for shorter measured lengths than for pure PVA samples, but the roughness for longer measured lengths is lower than for pure PVA

samples, which is explained by the lower Hurst number of the PVA-chitosan blend. The Hurst exponent and fractal dimension of the samples indicate a higher level of fractality, a more irregular shape of the surface topography for the PVA-chitosan films.

ACKNOWLEDGMENT

We acknowledge financial support from under project: Ref. 2022-GRIN-34226 (Plan Propio UCLM cofunded 85% by FEDER). G.K. acknowledges financial support from the UCLM for her stay in Almadén, Spain under contract 2022-UNIVERS-11036, ref. 2022-POST-20987.

REFERENCES

[1] P. Negi, G. Sharma, C. Verma, P. Garg, C. Rathore, Kulshrestha, U. Ranjan Lal, B. Gupta, D. Pathania, Novel thymoquinone loaded chitosan-lecithin micelles for effective wound healing: Development, characterization, and preclinical evaluation, Carbohydrate Polymers, V. 230, 2020, 115659

[2] E. Santini, E. Jarek, F. Ravera, L. Liggieri, P. Warszynski, M. Krzan, Surface properties and foamability of saponin and saponin-chitosan systems, Colloids and Surfaces B: Biointerfaces, V. 181, 2019, P. 198-206.

[3] Xiao-Yan Wang, Jun Wang, D. Rousseau, Chuan-He Tang, Chitosan-stabilized emulsion gels via pH-induced droplet flocculation, Food Hydrocolloids, V. 105, 2020, 105811.

[4] Mei Liu, Yibin Zhou, Yang Zhang, Chen Yu, Shengnan Cao, Preparation and structural analysis of chitosan films with and without sorbitol, Food Hydrocolloids, V. 33, Is. 2, 2013, P. 186-191.

[5] A. Rafique, K.M. Zia, M. Zuber, S. Tabasum, S. Rehman, Chitosan functionalized poly(vinyl alcohol) for prospects biomedical and industrial applications: a review, Int. J. Biol. Macromol., V. 87, 2016, P. 141–154.

[6] H. Chopra, S. Bibi, S. Kumar, M.S. Khan, P. Kumar, I. Singh, Preparation and evaluation of chitosan/PVA based hydrogel films loaded with honey for wound healing application, *Gels,* V. 8, 2022, 111.

[7] M. T. Cuberes, "Mechanical Diode-Based Ultrasonic Atomic Force Microscopies," in Applied Scanning Probe Methods XI. Nanoscience and Technology. Berlin, Heidelberg: Springer, 2009.

[8] Chengfu Ma, Walter Arnold, Nanoscale ultrasonic subsurface imaging with atomic force microscopy. *J. Appl. Phys.,* V. 128 (18), 2020, 180901.

[9] S. Marino, G. M. Joshi, A. Lusuardi, M. T. Cuberes, Ultrasonic force microscopy on poly(vinyl alcohol)/SrTiO3 nano-perovskites hybrid films, Ultramicroscopy, V. 142, 2014, P. 32-39.

[10] M.T. Cuberes, B. Stegemann, B. Kaiser, K. Rademann, Ultrasonic force microscopy on strained antimony nanoparticles, Ultramicroscopy, V. 107, Is. 10–11, 2007, P. 1053-1060.

[11] K. Lewandowska, Surface studies of microcrystalline chitosan/poly(vinyl alcohol) mixtures, Applied Surface Science, V. 263, 2012, P. 115–123.

[12] K. Lewandowska, Effect of an ionic liquid on the physicochemical properties of chitosan/ poly(vinyl alcohol) mixtures, International Journal of Biological Macromolecules, V. 147, 2020, P. 1156–1163.

[13] H. Assender, V. Bliznyuk, K. Porfyrakis, How Surface Topography Relates to Materials' Properties. Science, V. 297(5583), 2002, P. 973-976.

[14] I. Horcas, R. Fernández, J.M. Gómez-Rodríguez, J. Colchero, J. Gómez-Herrero and A.M. Baró. Review of Scientific Instruments, V. 78, 2007, 013705.

[15] P. Budrugeac. Kinetics of the complex process of thermo-oxidative degradation of poly(vinyl alcohol), Journal of Thermal Analysis and Calorimetry, V. 92, Is.1, 2008, P. 291–296

[16] M. Wisniewska, S. Chibowski, T. Urban, D. Sternik, Investigation of the alumina properties with adsorbed polyvinyl Alcohol, J. Therm. Anal. Calorim., V. 103, 2011, P. 329–337.

[17] V. Georgieva, D. Zvezdova, L. Vlaev. Non-isothermal kinetics of thermal degradation of chitosan, Chemistry Central Journal, 6, 81, 2012, P. 1-10.

[18] D. Johnson, N. Hilal, Polymer membranes – Fractal characteristics and determination of roughness scaling exponents, Journal of Membrane Science, V. 570–571, 2019, P. 9-22.

[19] 1D. Dallaeva, Ş. Ţălu, S. Stach, P. Škarvada, P. Tománek, L. Grmela, AFM imaging and fractal analysis of surface roughness of AlN epilayers on sapphire substrates, Applied Surface Science, V. 312, 2014, P. 81-86.

[20] E.C.T. Ba, M.R. Dumont, P.S. Martins, R.M. Drumond, M.P. Martins da Cruz, V.F. Vieira. Investigation of the effects of skewness Rsk and kurtosis Rku on tribological behavior in a pin-on-disc test of surfaces machined by conventional milling and turning processes. Mat Res, V. 24(2), 2021, e20200435.